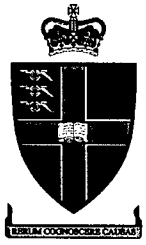

Cranfield UNIVERSITY

Defence College of Management and Technology

Department of Aerospace, Power & Sensors

TECHNICAL REPORT DAPS/ILM/115/2005

Ivor L. Morrow

September, 2005

Grant-04-3005

Final Progress Report: Launching of EM Surface Waves On Axial Cylindrical Reactive Surface with Negative Permittivity

REPORT DOCUMENTATION PAGE

Form Approved OMB No. 0704-0188

1. REPORT DATE *(DD-MM-YYYY)*	2. REPORT TYPE	3. DATES COVERED *(From – To)*
09-11-2005	Final Report	23 March 2004 - 23-Mar-05

4. TITLE AND SUBTITLE

Launching of Electromagnetic Surface Waves on Axial Cylindrical Reactive Surface with Negative Permittivity

5a. CONTRACT NUMBER
FA8655-04-1-3005

5b. GRANT NUMBER

5c. PROGRAM ELEMENT NUMBER

6. AUTHOR(S)

Dr. Ivor L Morrow

5d. PROJECT NUMBER

5d. TASK NUMBER

5e. WORK UNIT NUMBER

7. PERFORMING ORGANIZATION NAME(S) AND ADDRESS(ES)

Royal Military College of Science (RMCS), Cranfield University
Dept. of Aerospace, Power and Sensors
Swindon SN6 8LA
United Kingdom

8. PERFORMING ORGANIZATION REPORT NUMBER

N/A

9. SPONSORING/MONITORING AGENCY NAME(S) AND ADDRESS(ES)

EOARD
PSC 802 BOX 14
FPO 09499-0014

10. SPONSOR/MONITOR'S ACRONYM(S)

11. SPONSOR/MONITOR'S REPORT NUMBER(S)
SPC 04-3005

12. DISTRIBUTION/AVAILABILITY STATEMENT

Approved for public release; distribution is unlimited.

13. SUPPLEMENTARY NOTES

14. ABSTRACT

This report results from a contract tasking Royal Military College of Science (RMCS), Cranfield University as follows: The Grantee will investigate methods for reducing radar cross section of antennas. Specifically: 1.) Formulation of the antenna and waveguide launcher problem: (i) Define intra- and exterior-field forms on the antenna, (ii) define negative permittivity expressions appropriate to the medium composing the cylindrical radiator, for e.g., plasma or other electronic resonant media (meta-materials), (iii) formulate eigenfunction encompassing antenna and waveguide structure, and then determine (iv) the eigenvalues of the principal supported modes. 2.) Formulate solutions for the scattered fields by; (i) applying boundary conditions and (ii) decomposing the total field into its incident and scattered field component. 3) Derive functional theoretic transforms for the scattered fields. The likely mathematical steps will include (i) splitting the scattered field expressions into its bi-laterial Laplace equivalence and then (ii) Fourier transform expressions to z and/or w planes. 4.) Evaluate scattered field solutions via Wiener-Hopf integrals to determine (i) total average power transmitted to the surface, (ii) total average reflected and (iii) total power radiated, per unit incident power.

15. SUBJECT TERMS
EOARD, Physics, Antennas

16. SECURITY CLASSIFICATION OF:			17. LIMITATION OF ABSTRACT	18, NUMBER OF PAGES	19a. NAME OF RESPONSIBLE PERSON
a. REPORT	b. ABSTRACT	c. THIS PAGE			MICHAEL KJ MILLIGAN, Lt Col, USAF
UNCLAS	UNCLAS	UNCLAS	UL	24	19b. TELEPHONE NUMBER *(Include area code)* +44 (0)20 7514 4955

The investigation which is the subject of this Report was initiated by the Director of the Air Force Office of Scientific Research, Air Force Material Command, USAF and was carried out under the terms of grant/cooperative award number FA8655-04-1-3005.

Executive summary

This document is a deliverable for the study *Launching of Electromagnetic Surface Waves on Axial Cylindrical Reactive Surfaces with Negative Permittivity* under the grant/cooperative award no. FA8655-04-1-3005 and was issued by the EOARD.

In this, the final report, the excitation of the dominant TM surface wave on an axial reactive surface composed of a material of negative permittivity is again discussed using a different and more accurate analyses. Here we tackle the problem using a Wiener-Hopf treatment. The geometry is slightly modified from that described in the interim report to allow variation in some of the launcher parameters. The surface wave launcher now consists of a metallic cylindrical surface of radius b coaxial with a cylindrical rod of negative permittivity material of radius a, where $b \geq a$. The reactive surface extends from $l = -\infty < z < l$, and the conducting surface extends from $-\infty < z \leq 0$. The incident field is the dominant TM mode excited in the coaxial structure and propagating in the positive z-direction.

Numerical results are presented for the coupling of power to the surface wave, the reflected wave and the radiated field on the plasma rod. The calculations were performed over a wide range of ω_p/ω values. The case of waveguide excitation, i.e $b = a$, was compared were applicable with the results obtained using the two approximate aperture distributions. The case of coaxial excitation, i.e. $b > a$, was also briefly considered using the Wiener-Hopf analyses. The calculated launcher efficiency was shown to increase as the b/a ratio increased.

Contents

List of Figures

List of Tables

1 Introduction

1.1 Background

The problem of exciting surface waves on conventional dielectric rod antennas was widely treated in the 1960 and 70's literature. This extensive treatment was motivated largely by the inherently low attenuation and large bandwidth available in some surface wave launchers. An excellent survey on the types of surface waves and surface wave radiation useful in dielectric rod communication antennas has been collated by Chatterjee in [1, 2] and electrically small dielectric antenna by Luk [3]. Recently, researchers have returned to the subject with a view to constructing these antenna from novel dielectric and permeability materials that can support surface waves. These materials should be lightweight and robust and behave as anisotropic ferrite and/or plasma analogues. A knowledge of the properties of the surface wave and plasma material properties [4] associated with these structures can provide useful insight into their radiation mechanism and characteristics.

A common problem, whether using a conventional dielectric or otherwise, to host the surface and interior fields, is the efficient excitation or launching of the guided electromagnetic surface wave. A general requirement for a good surface wave launcher is a high launcher efficiency over a large bandwidth. As was pointed out in the interim report, when the surface wave fields are of infinite extent, the launcher in theory should also be of infinite extent to achieve a 100% launcher efficiency. Brown demonstrated theoretically [5] that the launching efficiency of a finite-sized launcher could approach 100%; but this large efficiency was realised only at the expense of frequency bandwidth.

The majority of reported numerical techniques consider the excitation source to be either infinitesimally short electric and/or magnetic dipole current sources. A finite-sized aperture could be handled, at least in theory, by a superposition of infinitesimal sources. In practice, the outcome has an unknown accuracy since the formulation fails to take account of the losses in the reflected field at the launcher. Secondly, because the aperture distribution may be unknown. In the interim report [6], the aperture distribution was approximated by a "chopped" surface wave distribution; that is, the fields in the aperture plane are assumed to have the same form as the surface wave fields within the aperture and are assumed to vanish everywhere outside of the aperture. Another often used approximation method is Kirchhoff's

approximation. In this method the aperture field is assumed to be of the same form as the unperturbed incident field. This distribution was also computed in the interim report [6] and the launcher efficiency results were found to be poorer than those obtained using the equivalent aperture technique. The principal reason for the discrepancy was attributed to the differing radiation patterns obtained as the ratio ω_p/ω was increased. The radiated fields were computed by both methods by an integration over the aperture plane (the surface wave modes and the radiation field are orthogonal [7]). The accuracy of the results obtained using these approximation techniques is usually unknown since no criterion exists which can determine the extent of the approximation.

1.2 Scope

The purpose of this report is to (i) present an exact analysis, using Laplace transform and Weiner-Hopf factorisation techniques (ii) and numerical results for the radiation pattern, bandwidth and launching characteristics for a finite-sized launcher. These results will then be compared with (iii) the results obtained in the interim report [6] for the "equivalent end-aperture" and Kirchhoff's approximations to determine under what conditions the approximate techniques are valid.

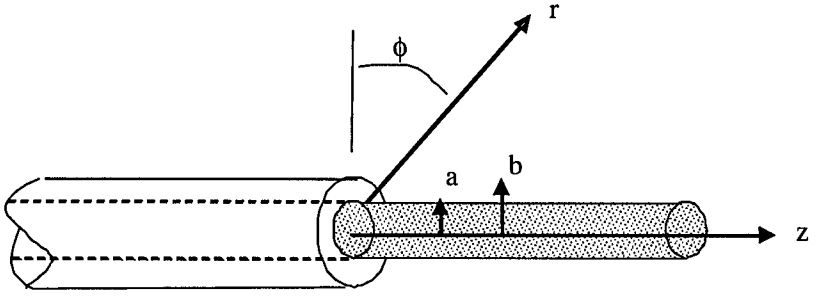

Figure 1: Surface Wave Structure.

A good deal of the ground work identifying the plasma cylinder dimensions, useful material properties and resonant eigenmodes was performed in [6]. The analysis considers the geometry shown in Fig. 1. The waveguide launching section has been modified from that in the interim report to allow for the possibility that $b > a$ i.e. coaxial excitation and when $b = a$, a cylindrical waveguide excitation as in the interim report. This modification has the

merit of generalising the analysis and design parameters but comes with an increased cost in analytic complexity. The surface wave field here is now taken account of by specifying a surface impedance. The surface impedance is the ratio of tangential electric to magnetic field on the surface of the wave guiding structure. This numerical value will depend on the composition of the structure and the polarisation of the propagating field.

The structure consists of a reactive negative permittivity cylindrical surface of radius a and of infinite extent in the z-direction. Coaxial with this cylinder is a thin, perfectly conducting surface of radius b for $z \leq 0$. The surface wave field, radiation field, and the reflected field will be computed when the incident field is the dominant TM_{00} mode in the region $a < r < b, z < 0$ propagating to the right. In this analysis the fields in the region $r < a$ are not needed and if they exist will not be considered in the calculations of power.

2 Modal Fields and Eigenfunctions

2.1 Coaxial Launcher for Axial Cylindrical Antenna

This problem can be handled with the Wiener-Hopf technique. The procedure to be followed is similar to that used by [8, 7]. The analysis will be carried out for a range in the parameters of the structure where only the dominant TM_{00} mode propagates in the region a $< r < b, z <$ 0. The total field in this case can be derived from a scalar function $\psi(r, z)$ because of the circular symmetry of the structure. The function $\psi(r, z)$ is the θ component of the magnetic field. In the region a $< r < b$ and $z < 0$, $\psi(r, z)$ can be expanded in a series of eigenfunctions [9, 10],

$$\begin{aligned}\psi(r,z) = A_0[&J_1(-jp_or)H_0^{(2)}(-jp_ob) \\ &-J_0(-jp_ob)J_1(-jp_or)H_0^{(2)}(-jp_or)]exp(-\gamma_o z) \\ +\textstyle\sum_{n=1}^{\infty} A_n[&J_1(p_nr)H_0^{(2)}(p_nb) \\ &-J_0(p_nb)H_1^{(2)}(p_nr)]exp(\gamma_n z) \end{aligned} \quad (1)$$

where the A_n are the propagation constants[1]. The J_0, J_1 represent Bessel functions of the first and second kind of zero and first order, and $H_0^{(1)}, H_0^{(2)}$ are Hankel functions of first

[1] A time dependence of $\exp(j\omega t)$ is assumed.

and second kind or order zero. The presence of a complex argument indicates the wave is attenuated, or augmented, in the outward traveling direction. The eigenvalues p_n and the propagation constant γ_n satisfy the equations

$$\gamma_0^2 = p_0^2 + k_0^2 \tag{2}$$

$$\gamma_n^2 = p_n^2 - k_0^2, \text{for } n > 0 \tag{3}$$

$$jp_0 a \frac{J_0(-jp_o b)H_0^{(2)}(-jp_o a) - J_0(jp_o a)H_1^{(2)}(-jp_o b)}{J_1(-jp_o a)H_0^{(2)}(jp_o b) - J_0(jp_o b)H_1^{(2)}(jp_o a)} = -\alpha a \tag{4}$$

$$p_0 a \frac{Y_0(p_n b)Y_0(p_n a) - J_0(p_n b)Y_0(p_n a)}{J_0(p_n b)Y_1(p_0 a) - J_1(p_n a)Y_0(p_n a)} = \alpha a, \text{for } n > 0 \tag{5}$$

$$\alpha = kX_s/Z_0 \tag{6}$$

where k_0 is the free-space wave number and Z_0 the characteristic impedance of free-space and Y_0, Y_1 are Bessel functions of the second kind or order zero and one. The eigenvalues p_n are determined by the boundary conditions. The ratio of the axial component of the electric field to the azimuth component of the magnetic field [11] must equal the surface reactance jX_s along the reactive surface at $r = a$. Along the surface of the perfect conductor $r = b$ the axial component of electric field must vanish. These conditions have been built into Eqn. 1. If surface reactance tends to zero, then the first term in Eqn 1 will reduce to the TM_{00} TEM like wave associated with a coaxial line and the remaining terms will reduce to the TM_{0n} modes for a coaxial line. Alternatively, if $b = a$, i.e. cylindrical waveguide excitation then the first term in Eqn. 1 reduces to zero and we are left with only the second term again permitting only the TM_{0n} modes, of which only the dominant TM_{01} is considered. It should be recalled that the total field consists entirely of TM_{0n} therefore it is only necessary to specify the surface reactance for one polarisation of the electric field.

2.2 Axial Cylindrical Antenna

The total field in the open antenna section consists of discrete modes guided by the reactive structure plus the radiated field. Since the field in the coaxial portion of the structure is made up entirely from circularly symmetric TM modes, then the field excited in the open structure must also be circularly symmetric, the only mode that possess circular symmetry is the TM_{01} mode.

The total field in the open structure consists of two components; the guided TM_{01} surface wave plus the radiated field. The surface wave must be of the form [12],

$$B_0 H_1^{(2)}(-jh_o r) = exp(-j\beta_0 z) \tag{7}$$

where B_0 is the complex amplitude constant. The eigenvalues h_0 and the propagation constant β_0 are related as,

$$\beta_0^2 = h_0^2 + k_0^2 \tag{8}$$

The eigenvalue h_0 satisfies the boundary eigenfunction equation obtained from Eqn 6.

$$jh_0 a \frac{H_0^{(2)}(-jh_0 a)}{H_1^{(2)}(-jh_0 a)} = \alpha a \tag{9}$$

The resulting eigenvalues and surface reactance values are consistent with those obtain from the approximate methods. The formal solution is now carried out using the Laplace transform and Wiener-Hopf techniques [11]. First, the total field $\psi(r,z)$ is decomposed into an incident $\psi_i(r,z)$ and scattered field $\psi_s(r,z)$ components,

$$\psi(r,z) = \psi_i(r,z) + \psi_s(r,z) \tag{10}$$

The incident field from the coaxial section of the structure will be of the form TM_0,

$$\psi_i(r,z) = \frac{\pi p_0 b}{2}[J_1(-jp_0 r)H_0^{(2)}(-jp_0 b) - J_0(-jp_0 b)H_1^{(2)}(-jp_0 r)]\exp(-j\gamma_0 z) \tag{11}$$

The scattered field beyond $z > 0$ satisfies Helmholt's equation expressed in cylindrical coordinates by Eqn. 12, the boundary conditions on the negative permittivity surface and the perfectly conducting surface are enforced by Eqns. 13 and 14, respectively. In addition the scattered field must also conform to the radiation condition, which requires solutions for the scattered field to be divergent waves at infinity.

$$\frac{\delta^2\phi_s}{\delta r^2} + \frac{1}{r}\frac{\delta\phi_s}{\delta r} + \frac{\delta^2\phi_s}{\delta r^2} + (k_0^2 - 1/r^2)\phi_s = 0 \tag{12}$$

$$\frac{1}{r}\frac{1}{\delta r}(r\phi_s) + \alpha\phi_s \mid_{r=a} = 0 \tag{13}$$

$$\frac{1}{r}\frac{1}{\delta r}(r\phi_s) \mid_{r=b,z<0} = 0 \tag{14}$$

2.3 Laplace Transformation of Scattered Field

The scattered field can be expressed as a bi-lateral Laplace transform along with the associated boundary conditions,

$$\phi(r,\beta) = \phi^+(r,\beta) + \phi^-(r,\beta) \tag{15}$$

where,

$$\phi^+(r,\beta) = \int_0^\infty \phi(r,z)\exp(-\beta,z)dz \tag{16}$$

$$\phi^-(r,\beta) = \int_{-\infty}^0 \phi(r,z)\exp(-\beta,z)dz \tag{17}$$

The scattered field can then be recovered by the inversion integral,

$$\psi(r,z) = \frac{1}{2\pi j}\oint \phi(r,\beta)\exp(\beta,z)d\beta \tag{18}$$

To make $\phi^+(r,\beta)$ and $\phi^-(r,\beta)$ analytic functions of β in the complex β region, the free space wave number k_0 will be made complex. This is equivalent to introducing losses into the medium surrounding the structure. Let $jk_0 = jk_0' + k_0''$, where k_0' and k_0 are real. In the final solution k_0'' can be made equal to zero to recover the results for the lossless case. Since k_0 is complex, the propagation constant γ_0 and β_0 will be complex. Therefore, in general $j\gamma_0 = j\gamma' + j\gamma_0''$ and $j\beta_0 = j\beta_0' + \beta_0''$. It should be remembered that $\beta_0', \beta_0'', \gamma_0'$ and γ_0'' are all real.

Taking the Laplace transform of Eqns. 12, 13 and 14 yields,

$$\frac{\delta^2\phi}{\delta r^2} + \frac{1}{r} + (\beta^2 + k_0^2 - 1/r^2)\phi = 0 \tag{19}$$

$$\frac{1}{r}\frac{1}{\delta r}(r\phi) + \alpha\phi \mid_{r=a} = 0 \tag{20}$$

$$\frac{1}{r}\frac{1}{\delta r}(r\phi^-) + \alpha\phi \mid_{r=b} = 0 \tag{21}$$

where β is restricted to the range $-\gamma_0'' < Re(\beta) < \gamma_0''$.

2.4 Solution of Transformed Scattered Field

In the region $a < r < b$ the proper solution of Eqn. 19 is of the form,

$$\psi(r,\beta) = \psi(b^-,\beta)\frac{[\lambda H_0^{(2)}(\lambda a) + \alpha H_1^{(2)}(\lambda a)]J_1(\lambda r) - [\lambda J_0(\lambda a) + \alpha J_1(\lambda a)]H_1^{(2)}(\lambda r)}{[\lambda H_0^{(2)}(\lambda a) + \alpha H_1^{(2)}(\lambda a)]J_1(\lambda b) - [\lambda J_0(\lambda a) + \alpha J_1(\lambda a)]H_1^{(2)}(\lambda b)} \tag{22}$$

The solution is an even function of λ consequently either branch of λ can be selected. In the region $r > b$ the proper solution of Eqn. 19 is,

$$\psi(r,\beta) = \psi(b^+,\beta)\frac{H_1^2(\lambda,r)}{H_1^2(\lambda,b)} \tag{23}$$

where $\lambda = (k_0^2 + \beta^2)^{1/2}$. We will now determine expressions for the unknown coefficients $\phi(b^-,\beta)$ and $\phi(b^+,\beta)$ in Eqns. 22 and 23 by using the discontinuity condition on the scattered field at $r = b$. This is achieved using some auxiliary functions $J^+(b,\beta)$, $J^-(b,\beta)$ and $E^+(b,\beta)$, where

$$J^+(b,\beta) = \int_0^\infty [\psi_s(b^+,z) - \psi(b^-,z)]\exp(-\beta z)dz \tag{24}$$

$$J^-(b,\beta) = \int_{-\infty}^0 [\psi_s(b^+,z) - \psi(b^-,z)]\exp(-\beta z)dz \tag{25}$$

$$E^+(b,\beta) = \frac{1}{r}\frac{\delta}{\delta r}(r\psi) \mid_{r=b} \tag{26}$$

Is should be mentioned that $J^-(b,\beta)$ is the Laplace transform of the electric current on the outer conductor of the coaxial guide at $r = b$ associated with the scattered field. The function $E^+(b,\beta)$ is the transform of the axial component of the total electric field evaluated

at $r = b$. The function $J^+(b,\beta)$ can be deduced for the region $Re(\beta) > -\gamma_0''$ by consideration of the boundary conditions.

$$J^+(b,\beta) = \frac{1}{\beta + j\gamma_0} \tag{27}$$

From the definitions of $J^+(b,\beta)$ and $J^-(b,\beta)$ it is apparent that

$$\phi(b^+,\beta) - \phi(b^-,\beta) = J^+(b,\beta) - J^-(b,\beta) \tag{28}$$

The left side of Eqn. 29 may be reduced to,

$$\phi(b^+,\beta) - \phi(b^-,\beta) = F(\beta)E^+(b,\beta) \tag{29}$$

where $F(\beta)$ after analytic manipulation is explicitly written out to give,

$$F(\beta) = \frac{2j}{\pi b\lambda^2}\frac{H_0^{(2)}(\lambda a)}{H_0^{(2)}(\lambda b)}\left[\lambda + \alpha\frac{H_1^{(2)}(\lambda a)}{H_0^{(2)}(\lambda a}\right] \times \tag{30}$$
$$\frac{1}{\lambda[H_0^{(2)}(\lambda a)J_0(\lambda b) - H_0^{(2)}(\lambda b)J_0(\lambda a)] + \alpha[H_0^{(2)}(\lambda a)J_0(\lambda b) - H_0^{(2)}(\lambda b)J_1(\lambda a)]}$$

The function $F(\beta)$ can be shown to be analytic in the strip $-\gamma_0'' < Re(\beta) < -\gamma_0''$. Substituting Eqn. 29 into Eqn. 31 and using the result for $J^+(b,\beta)$ from Eqn. 28 gives,

$$F(\beta)E^+(b,\beta) = J^-(b,\beta) + \frac{1}{\beta + j\gamma_0} \tag{31}$$

2.4.1 Wiener-Hopf Factorisation

Eqn. 31 can be solved for the functions $E^+(b,\beta)$ and $J^-(b,\beta)$ by performing a Wiener-Hopf factorisation on the function $F(\beta)$; i.e. $F(\beta)$ will be expressed as the ratio of the two functions $F^+(\beta)$ and $F^-(\beta)$, where F^+ is analytic and nonzero for $Re(\beta) > \gamma_0''$ and F^- is analytic and non-zero for $Re(\beta) < \gamma_0''$. Some of the important properties of the functions are listed below;

- The function $F^+(\beta)$ has a single zero at $\beta = -j\beta$ and a branch point at $\beta = -jk_0$.

- The function $F^-(\beta)$ has an infinite number of zeros in the complex β-plane and a branch point at the $\beta = jk_0$. The zeros of $F^-(\beta)$ are located at $\beta = j\gamma_0$ and $\beta = \gamma_n (n > 0)$.
- The function $F^+(\beta)$; is of the order $\beta^{-1/2}$ at infinity, and the function $F^-(\beta)$ is the order $\beta^{-1/2}$.

The decomposition of the function $F(\beta)$ into the ratio of $F^+(\beta)$ to $F^-(\beta)$ means we can transform Eqn. 31 to,

$$F^+(\beta)E^+(b,\beta) = \frac{F^-(-j\gamma_0)}{\beta + j\gamma_0} = \frac{F^-(\beta) - F^-(-j\gamma_0)}{\beta + j\gamma_0} - F^-(\beta)J^-(b,\beta) \tag{32}$$

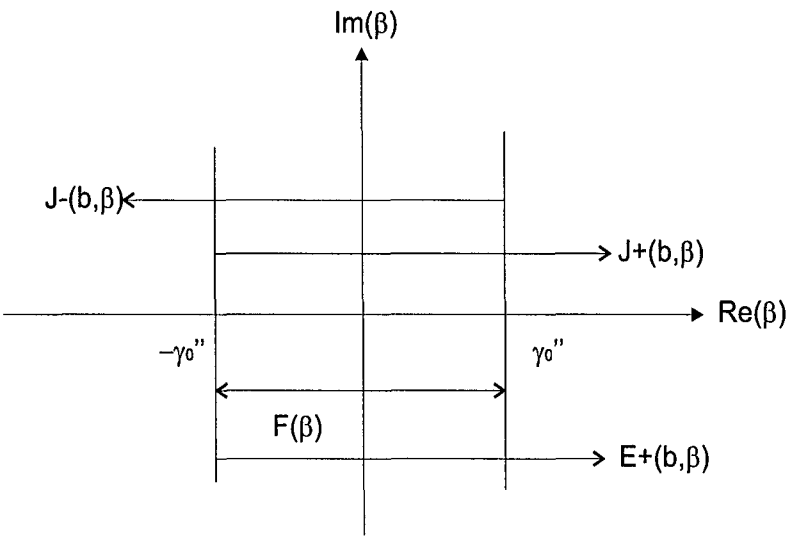

Figure 2: Complex plane diagram illustrating the areas were the various transforms are analytic.

Fig. 2 shows the complex β-plane and illustrates the boundaries of the various analytic functions. For the solution of the scattered field to be unique conditions on the edge or boundary must be enforced at $r = b$ and $z = 0$. These conditions require the axial component of the electric field to be of the order of $z^{1/2}$ at the edge, which makes the transform of the electric field (i.e., $E^+(b,\beta)$) of the order of $\beta^{-1/2}$ as $\beta \to \infty$. Similar conditions exist for the asymptotic form of the current at the edge. This condition requires $J^-(b,\beta)$ to be of the

order of β^{-1} as $\beta \to -\infty$. Applying Lioville's theorem to enforce edge conditions, Eqn. 32 can be equated to zero, which yields;

$$E^+(b,\beta) = \frac{F^-(-j\gamma_0)}{F^+(\beta)(\beta + j\gamma_0)} \tag{33}$$

2.4.2 Scattered Field Inversion Integral

The coefficient $\psi(b^+,\beta)$ can now be expressed in terms of the known function $E^+(b,\beta)$ by using Eqns. 22,23, and 26,

$$\psi(b^-,\beta) = \frac{H_1^{(2)}((k_0^2+\beta^2)^{1/2}b)F^-(-j\gamma_0)}{(k_0^2+\beta^2)^{1/2}H_0^{(2)}((k_0^2+\beta^2)^{1/2}b)F^+(\beta)(\beta+j\gamma_0)} - \frac{F^-(-j\gamma_0)}{F^-(\beta)(\beta+j\gamma_0)} \tag{34}$$

The scattered magnetic field, $\psi(r,z)$, may now be computed by using the inversion integral,

$$\psi(r,z) = \frac{1}{2\pi j}\int_c \phi(r,\beta)\exp(\beta z)dz \tag{35}$$

The inversion contour C is shown in Fig. 3 and must be located in the strip $-\gamma_0'' < Re(\beta) < \gamma_0''$ and be on the sheet of the Riemann surface that corresponds to the choice $\mathrm{Im}(k_0^2+\beta^2)^{1/2} < 0$ in the strip. The branch cuts are selected as radial straight lines starting from the branch points $\beta = \pm jk_0$. For the lossless case the branch cuts are located on the imaginary β axis.

To compute the discrete spectrum, the amplitude of the modes must be evaluated at only one radius. It seems sensible to evaluate the field at the radius $r = b$ since the radial varying factor of the general solutions are normalised to unity at $r = b$.

Taking the region $a < r < b$ and $z < 0$, the amplitude of the scattered field at $r = b$ is,

$$\psi(b,z) = \frac{1}{2\pi j}\int_c \psi(b^-,\beta)\exp d(\beta z)dz \tag{36}$$

where $\psi(b^-,\beta)$ is given by equation Eqn. 35. The contour C is closed in the right half of the β-plane with a semi-circle of infinite radius deformed around the branch cut as shown

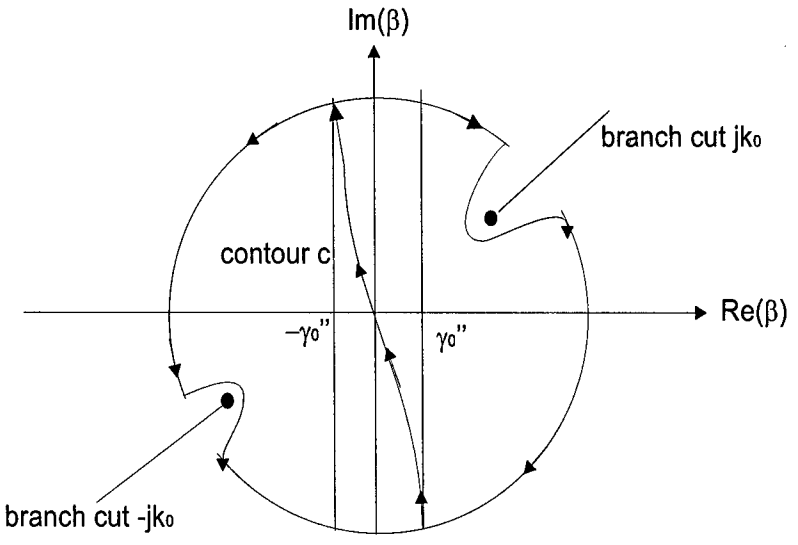

Figure 3: The Inversion Contour in the Complex Plane.

in Fig. 3. The details of the integration are omitted for brevity, but are based upon the technique outlined in Chapter 4 of [13], for integration of isolated saddle points. Suffice to say the integration along the semi-circle and along the branch cut can be shown to be zero for $z < 0$. Thus, the integral over the original contour must equal $2\pi j$ times the sum of the residues of the enclosed poles in the right half β plane. All the poles of the $\psi(b^-, \beta)$ in the right half are due to the zeros of the $F^-(\beta)$. Therefore,

$$\psi_s(b,z) = \frac{F^-(-j\gamma_0)}{2j\gamma_0 \frac{\delta F^-(\beta)}{\delta(\beta)}\,|_{\beta=j\gamma_0}} \exp(j\gamma_0 z) + \sum_{n=1}^{\infty} \frac{F^-(-j\gamma_0)}{(\gamma_n + j\gamma_0)\frac{\delta F^-(\beta)}{\delta(\beta)}\,|_{\beta=j\gamma_n}} \exp(\gamma_n z) \qquad (37)$$

The first term of Eqn. 37 represents the dominant TM_{00} coaxial mode in the reflected field and the summation represents the evanescent TM_{0n} modes in the reflected field. For $z << 0$ the reflected field consists entirely of the first term, the TM_{00} mode.

The field in the region $z > 0$ evaluated at $r = b$ can be found by using the same inversion integral. This time the contour is closed in the left half of the β plane with a semi-circle of infinite radius that is deformed around the the branch cut. The integration along the semi-circle can be shown to be zero for $z > 0$. Therefore, the integral must equal $2\pi j$ times the sum of the residues of the enclosed poles in the left half β plane plus the branch cut integral. The poles of $\psi(b^-, \beta)$ in the left half β plane are due to the zeros of $F^+(\beta)$ at

$r = j\beta_0$ and the pole appearing explicitly in Eqn. 35 at $\beta = -j\gamma_0$. Thus for $z > 0$,

$$\psi_s(b,z) = \frac{F^-(-j\gamma_0) - jH_1^{(2)}(-jk_0b)}{(k_0^{2'} - \beta_0^2)^{1/2}H_0^{(2)}(-jk_0b)(\gamma_0 - \beta_0)\frac{\delta F^-(\beta)}{\delta(\beta)}\,|_{\beta=j\beta_0}} \exp(j\beta_0 z) \qquad (38)$$
$$+ \exp(-j\gamma_0 z) + \text{branch cut integral}$$

The first term in Eqn. 39 represents the TM_{01} surface wave mode in the open section of the antenna. The second term is the scattered field which nulls the incident field in the region $z > 0$.

The branch cut integral or continuous part of the spectrum gives rise to the waves associated with the radiated field. The pattern of the far zone radiated field is evaluated approximately by the saddle point method of integration, the contour C is deformed into a contour of steepest descent. Transforming r and z from cylindrical to a spherical co-ordinate frame with the orientation given in Fig. 1 the expression for the far-field radiation is,

$$\psi_s(\rho,\phi) = \frac{F^-(-j\gamma_0)\exp -j(k_0\rho + \pi/2)}{\pi F^+(-jk\sin\phi)(H_0^{(2)}(kb\cos\phi))(\gamma_0 - k\sin\phi)(k\rho\cos\phi)} \qquad (39)$$

The total field can now be found by adding the scattered field to the incident field as given in Eqn. 10.

3 Power Flow and Antenna Efficiency

The energy transported by the field is computed using the Poynting theorem. The only components of the total field that transport energy are the TM_{00} incident field (Eqn. 11), the TM_{00} reflected field (first term of 37), the TM_{01} surface wave field (first term of Eqn. 39) and the radiated far field, Eqn. 39. $\psi(r,z)$ is the θ component of the total magnetic field, the electromagnetic fields $\vec{E}, \vec{H}$ are given by,

$$\vec{E} = \frac{1}{j\omega\epsilon_0}\nabla \times \psi\hat{a_\theta} \qquad (40)$$
$$\vec{H} = \psi\hat{a_\theta}$$

Thus the power associated with the total field is,

$$\vec{P} = 1/2\mathrm{Re}\int_s \vec{E} \times \vec{H}^* \cdot ds \tag{41}$$
$$= \frac{1}{2\omega\epsilon_0}\mathrm{Im}\int_S (\nabla \times \psi\hat{a_\theta}) \times \psi^* \hat{a_\theta} \cdot ds$$

where ψ^* denotes the complex conjugate and s is a surface normal to the surface wave. For the case of the incident, reflected and surface wave fields, the only component of the curl of $\psi\hat{a_\theta}$ that is of interest is the radial component given by $-\delta\psi/\delta z$. The power guided, reflected and radiated are therefore,

$$P_{inc} = \frac{\pi\gamma_0}{\omega\epsilon_0}\int_a^b |\psi_i|^2 r dr \tag{42}$$

$$P_{ref} = \frac{\pi\gamma_0}{\omega\epsilon_0}\int_a^b |\psi_r|^2 r dr \tag{43}$$

$$P_{surf} = \frac{\pi\gamma_0}{\omega\epsilon_0}\int_a^b |\psi_s|^2 r dr \tag{44}$$

where the subscripts refer to the incident, reflected and surface wave components, respectively, of the total field. For the case of the radiated field the component of $\psi\hat{a_\theta}$ that is of interest is given by $\frac{1/\rho}{\delta/\delta\rho}(\rho\phi)$. The power radiated is therefore,

$$P_{rad} = \frac{\pi k_0}{\omega\epsilon_0}\int_{-\pi/2}^{\pi/2} |\psi_{rad}|^2 \rho^2 \cos\phi d\phi \tag{45}$$

As defined in the the interim report the quality of the surface wave launcher is computed from the definition of launcher efficiency as a function of frequency. The launcher efficiency was defined in [6] as the ratio of the surface wave to the total power radiated from the aperture of the launcher.

$$\eta_{laun} = \frac{P_{flow}(r \leq a)}{P_{flow}(r \leq a) + P_{flow}(r > a)} \tag{46}$$

This calculation also provides an opportunity to check the validity of the two approximate techniques calculated for the TM_{01} mode against the results of an exact analysis.

4 Computed Results

Results were computed for the case of the cylindrical waveguide launcher with the same dimensions and plasma parameters used in the interim report (i.e., $\lambda = 60.0cm, l = 3.0cm$ and $a = 0.1cm$). To replicate the excitation of the plasma rod from cylindrical waveguide $b/a = 1$.

The eigenvalues, radiated fields and power transport for the principal TM_{01} mode were computed. This was performed on the Dell Precision 360 Workstation using the Matlab programming language. Matlab possesses several very useful features; the Bessel and Hankel functions used were "built in" and conform to those most frequently used by engineers [14], it automatically selects the principal value of an analytic function and lastly has a toolbox that can handle steepest descent integrations. Table 1 shows the computed permittivity and surface impedances of the harmonic cylindrical fields over the same ratios of ω_p/ω used in the interim report. The values are in close agreement with those calculated in the interim report.

Plasma Freq Ratio (ω_p/ω)	Permittivity (F/m)	Surface Impedance (Ω)
5.4	-28.1	j71.1
9.0	-81.2	j42.0
100	$-10,000$	j3.7
10^5	-1.1×10^{11}	$\approx$ j0

Table 1: Table of Surface Impedance versus Plasma frequency ratios at $r = a$ for TM_{01} mode on the plasma rod ($\lambda = 60$ cm, $l = 3.0$ cm, $a = 0.1$ cm).

4.1 Radiated Fields

Figs. 4 and 5 show the radiated fields from the launcher for the case $b/a = 1$ and ω_p/ω values corresponding to those given in Table 1. (The curves have been normalised to the maximum value of the power density to aid comparison with those in the interim report). The figure illustrates how the radiated field changes for different values of surface reactance or equivalently negative permittivity. The field pattern shape changes with increasing negative

permittivity, which are in broad agreement with those predicted in the interim report by the equivalent two-aperture end fire analysis, although there are some subtle differences that begin to emerge when $\omega_p/\omega > 10^2$. The most notable difference is the presence of a small broadside lobe in the main beam when $\omega_p/\omega = 10^5$. It appears likely that another mode, probably the HE_{11}, is being partially excited, propagated and radiated; and some of this energy has been picked up in the radiation contour integration. The inference drawn in the interim report is verified here that the approximate equivalent aperture analysis method took more precise account of the fields present than the Kirchhoff method.

4.2 Power Propagated and Radiated

The results for the powers propagated and radiated are shown in Fig. 6, for a value of $\nu/\omega = 0.01$. Where ν is the collision frequency in the plasma and ω the radian rf excitation frequency[2]. The ratios of forward traveling (z directed) surface wave power, reflected power, and radiated power to the incident power are given in percentage terms as a function of ω_p/ω over the usual range. The results show that the waveguide launcher is efficient in launching the TM_{01} surface wave and as the ratio ω_p/ω increases the reflected power decreases.

4.3 Waveguide Launcher Efficiency

Fig. 7 shows the launching efficiency vs ω_p/ω for the structure calculated based on the "chopped" surface wave distribution. The Wiener-Hopf result is presented along with the results obtained for the equivalent end aperture and Kirchhoff surface methods. The launching characteristics both exact and approximate have the same general behavior as shown in Fig. 7. Closer inspection indicates the Wiener-Hopf consistently predicts higher launching efficiency than those computed using the approximate methods. This feature if carried over to a practical antenna design would deliver less losses. With regard performance bounds, the approximate methods yield quite accurate results over the range $10^{-1} \leq \omega_p/\omega \leq 10^1$. Beyond this point the Wiener-Hopf results diverge from the approximate and this is thought to be commensurate with the decrease in reflected power shown in Fig. 6.

[2]these terms and their relationship to the plasma frequency ω_p and permittivity ϵ_r were described in the interim report.

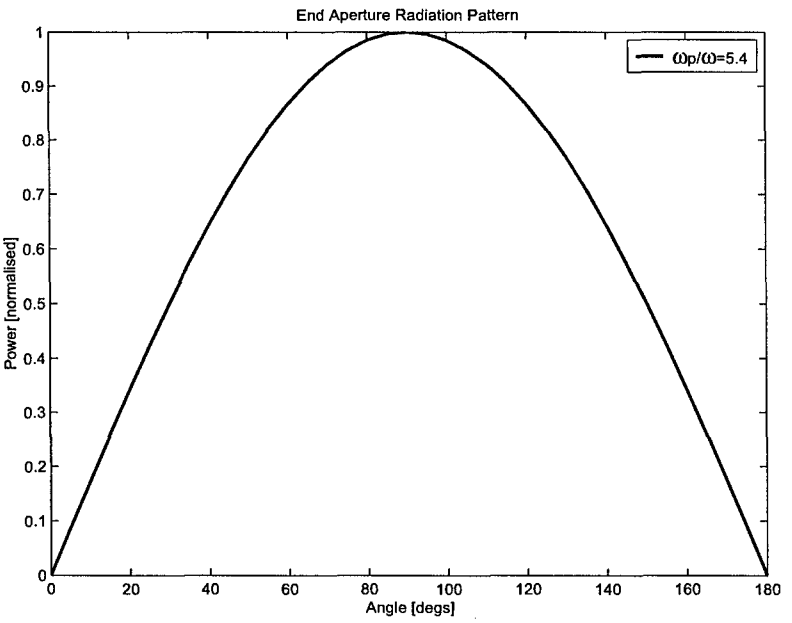

(a)

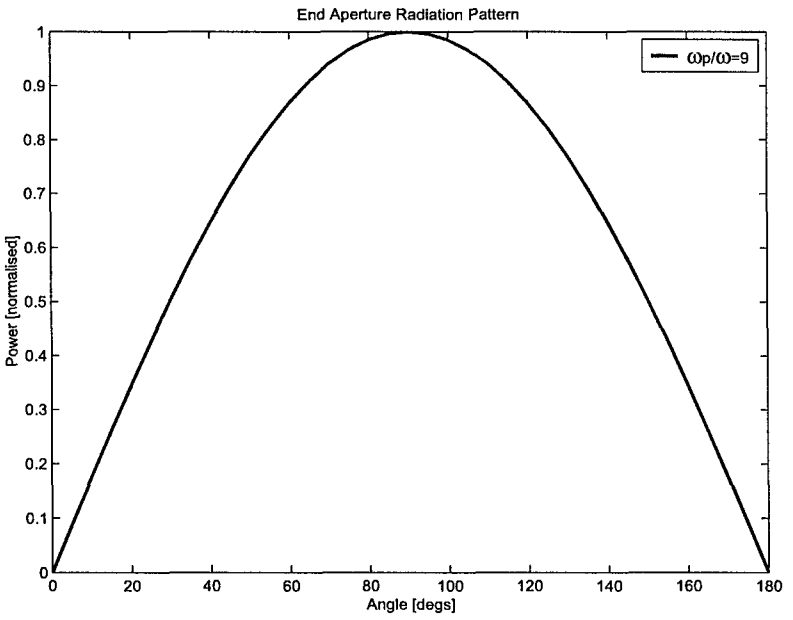

(b)

Figure 4: Radiation pattern due to fields on the radial surface of the cylindrical plasma supporting the TM_{01} mode for various ω_p/ω ratios.(a) $\omega_p/\omega = 5.4$ (b) $\omega_p/\omega = 9.0$.

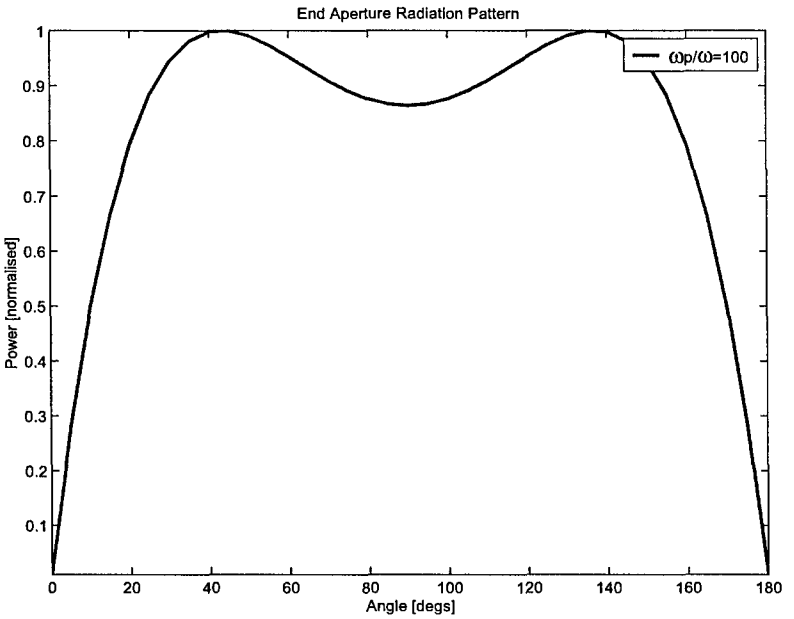

(c)

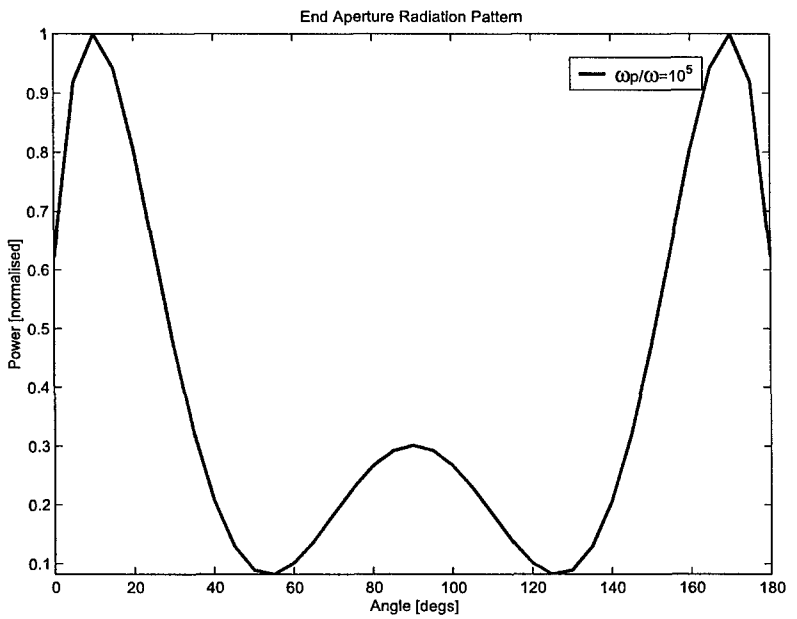

(d)

Figure 5: (Contn). Radiation pattern due to fields on the radial surface of the cylindrical plasma supporting the TM_{01} mode for various ω_p/ω ratios.(c) $\omega_p/\omega = 100$ (d) $\omega_p/\omega = 1\times10^5$.

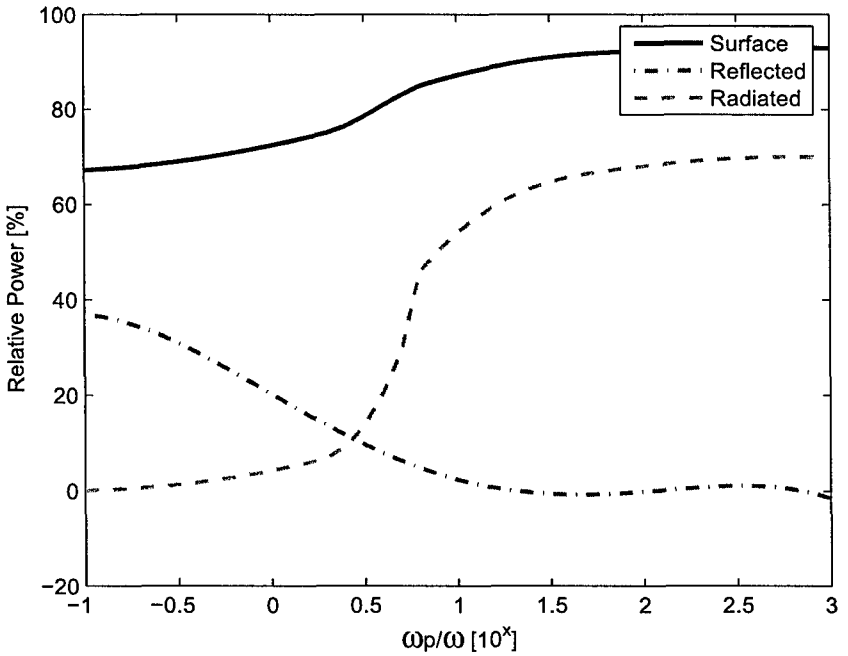

Figure 6: Ratio of Powers Coupled from the Incident wave to the forward travelling Surface Wave, Reflected Surface Wave and Radiated Field for the TM_{01} mode.

4.4 Coaxial Launcher Efficiency

In studying a specific design of launcher, i.e. the waveguide launcher, we were able to determine that a modestly efficient, electrically small plasma antenna was practically feasible. However other forms of launcher do exist which might deliver higher coupled powers to the antenna. Perhaps, the most effective of which is a coaxial launcher. Since by varying the inner to outer ratio of the radius of the plasma rod to metallic cylinder we can vary the impedance matching between the propagating and radiating wave-fields (as suggested in Section 1.2).

The outer radius b was increased to a ratio of $b/a = 2.3$. The ratios of 2.3 corresponds to a coaxial characteristic impedances of 50Ω and is not intended to be an optimum impedance match over the whole range of plasma ratios. It is, however, intended to provide some impedance matching over the critical region of the antennas operation i.e., $10^1 < \omega_p/\omega < 10^2$. Fig. 8 compares the results for the launching efficiency of the waveguide and coaxial

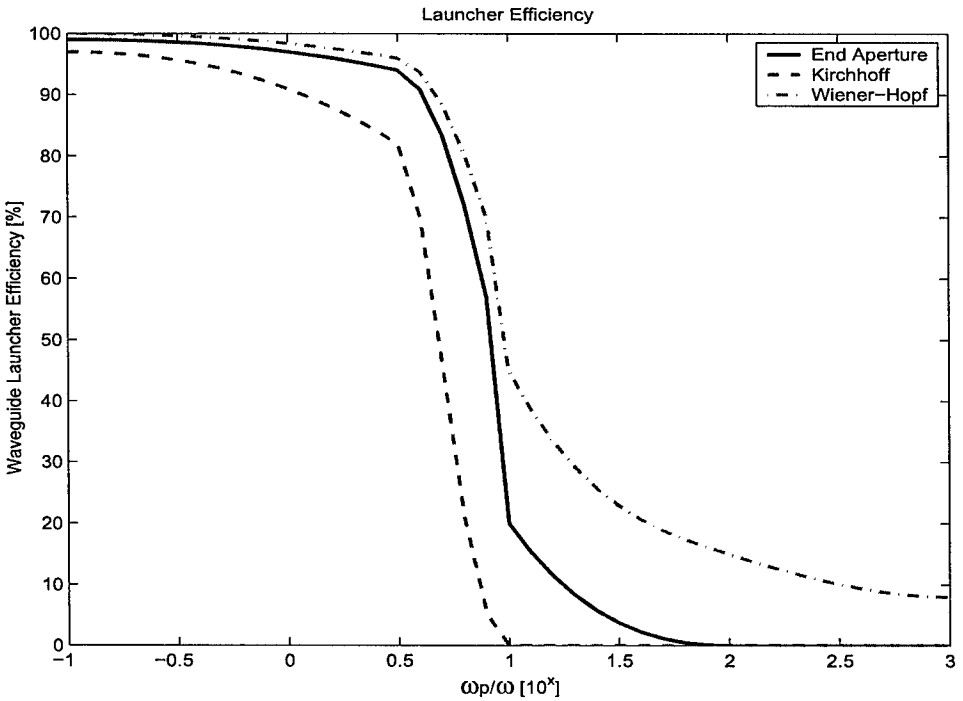

Figure 7: Computed Launcher Efficiency for Cylindrical Waveguide Excitation with the TM_{01} mode using the End aperture, Kirchhoff and the Wiener-Hopf methods.

launchers. From the figure it is clear their is no significant improvement below $\omega_p/\omega < 1$, beyond this region the launching efficiency is observed to increase slightly.

5 Conclusions

An antenna composed of a negative permittivity material and excited via a waveguide launcher has been investigated mathematically. Two independent treatments of the problem have been given; In the interim report two approximate analyses using the Kirchhoff and equivalent end aperture method were applied and in this report an exact method, using the Wiener-Hopf technique developed. The exact solution provides results with bounded accuracy and are considered more rigorous.

- The launcher efficiency was computed for all three methods based upon the "chopped surface wave" definition. On the approximate methods, the equivalent end aperture

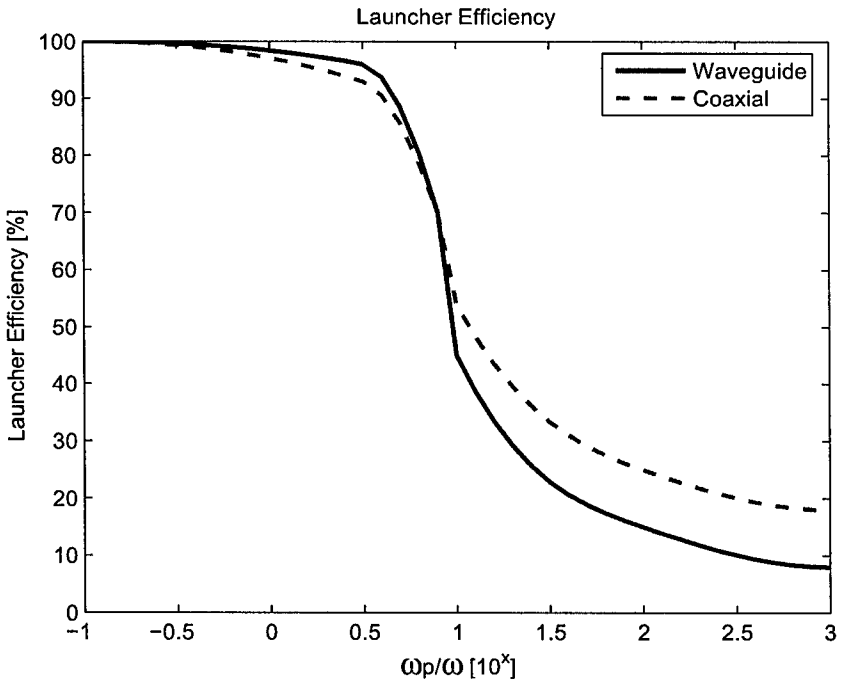

Figure 8: Computed Launcher Efficiency for Cylindrical Waveguide and Coaxial Excitation (waveguide $b/a = 1$, coaxial $b/a = 2.3$).

results were more accurate than the Kirchhoff solution when compared with the Wiener-Hopf solution.

- Both Wiener-Hopf and end aperture analyses indicate the possibility for constructing an electrically small antenna from a negative permittivity material that is fairly radiation efficient. The analyses here further endorses the summary conclusion made in the interim report.

- The Wiener-Hopf solutions consistently calculated slightly higher launching efficiencies up to $\omega_p/\omega = 10^1$ and beyond this point did not cut off. One reason suggested for this behaviour is when $\omega_p/\omega \geq 10^1$, the internal fields are being gradually occluded from the interior plasma and energy transport is occurring only on the surface, were the impedance losses are low. In the approximate methods losses were assumed and computed throughout the cross-section of the interior guide.

- For completeness a coaxial launcher design was also investigated. This was demonstrated to provide more effective matching of the launcher to the plasma geometry. The results indicate that this could enhance launcher efficiency by another 10% for $\omega_p/\omega \geq 1$. As the plasma ratio increases the radiation patterns followed the waveguide behaviour.

6 Recommendations for Future Work

The following recommendations are made;

- It would seem appropriate to experimentally substantiate some of the claims made in the conclusions. This could be achieved via another cooperative research program. Reported experiments with negative permittivity antennas have concentrated on free-space plasmas [15, 16]. However, these antenna suffers from high losses and present many practical implementation issues. The idea proposed here is to construct a passive plasma analogue material[3], excite it using the coaxial launcher and characterise its performance. The intended operating band would be in the 20-1000 MHz frequency spectrum were compact, lightweight wideband aerials for mobile communications are often required. Transmit power would be restricted to a few 10's of Watts. A single antenna is suggested were the engineering novelty should be to provide an antenna much more compact than a conventional $\lambda/4$ or $\lambda/2$ whip aerial.

- It is unlikely that a single antenna will be suitable to cover the whole frequency spectrum mentioned above. Therefore, I should wish to extent the research effort to either compact clustered or active plasma analogue variants. This latter effort would address the challenge of achieving more bandwidth and/or more gain. AFRL should advise if such a study is relevant to their current requirements and how best to initiate the study.

- One other attendant research issue is the antenna operation. The radiation from any electrically small HF antenna, which is dipole like, will be effected by the presence of

[3]Some interesting papers were highlighted in the Interim Report that point to useful passive negative permittivity materials that may be suitable for antenna application.

the equipment operator, the ground and surrounding environment. It would also be appropriate to investigate experimentally, or otherwise, the effect on radiation pattern and antenna system losses in the vicinity of dielectric and conductive objects.

- To make appropriate conference and journal publications based on this work and citing the EOARD sponsorship. It is noted there has been a recent call for a special issue of the IEE on metamaterials and novel antennas.

—ooOoo—

7 Acknowledgements

The author would like to acknowledge Profs. J. R. James and J. S. Dahele for many stimulating and interesting conversations on many aspects of the theory, design and practice with dielectric and material loaded antenna structures. I should particularly like to thank Prof. Jash Dahele for the generous grift of his collection of electromagnetic texts and research papers. I also should like to personally congratulate Jash on his award of Emeritus Professor.

8 References

[1] R. Chatterjee. *Dielectric and Dielectric-Loaded Antennas.* Research Studies Press Ltd., Wiley and Sons, 1985.

[2] C. Salema, C. Fernandes, and R. K. Jha. *Solid Dielectric Horn Antennas.* Artech House, 1998.

[3] K. Man Luk and K. Leung. *Dielectric Resonator Antennas.* Research Studies Press Ltd., 2003.

[4] J. R. Wait. *Electromagnetics and Plasmas.* Holt, Rinehart and Winston, 1968. Chapter 5.

[5] J. Brown. Some theoretical results for surface wave launcher. *IEE Trans. on Antennas and Propagat.*, pages pp. 169–174, December, 1959.

[6] I. L. Morrow. Interim progress report: Launching of electromagnetic surface waves on axial cylindrical reactive surfaces with negative permittivity. Technical Report DAPS/ILM/113/2005, Cranfield University, RMCS, Shrivenham, Swindon, Wilts. UK, SN6 8LA, June 2005.

[7] R. E. Collins. *Field Theory of Guided Waves.* IEEE Press, 2nd edition edition, 1991. Chapter 11.

[8] C. M. Angulo and W. Chang. The excitation of a dielectric rod by a cylindrical waveguide. *IRE Trans. on Microwaves Theory and Techniques*, pages pp. 389–393, Oct. 1958.

[9] D. S. Jones. *Acoustic and Electromagnetic Waves.* Oxford University Press, 1986.

[10] P. M. Morse and H. Feshback. *Methods of Theoretical Physics.* McGraw-Hill, 1953.

[11] J. A. Stratton. *Electomagnetic Theory.* McGraw-Hill, 1941.

[12] H. M. Barlow and J. Brown. *Radio Surface Waves.* Oxford University Press, London, 1962.

[13] L. B. Felsen and N. Marcuvitz. *Radiation and Scattering of Waves.* IEEE Press, 1994.

[14] Abramowitz and Stegun. *Handbook of Mathematical Functions.* Dover Publications, Inc. New York, June 1964.

[15] G. G. Borg and J. H. Harris. Application of plasma columns to radio frequency antennas. *Applied Physics letters*, 74:3272–3274, 1999.

[16] G. G. Borg, J. H. Harris, N. M. Martin, D. Thorncraft, R. Miliken, D. G. Mijak, B. Kwan, T. Ng, and J. Kircher. Plasmas as antennas: Theory, experiment and applications. *Physics of Plasmas*, 7:2198–2202, 2000.